15th IFK
Proc. of the 15th International Fluid Power Conference <Symposium/Conference>
<DOI>

Performance analysis of rotary mechanical pulsation compensators for different types of pumps

Gudrun Mikota[1], David Holzer[2]

Institute of Machine Design and Fluid Power, Johannes Kepler University Linz, Altenbergerstrasse 69, A-4040 Linz, Austria, [1]gudrun.mikota@jku.at, [2]david.holzer@jku.at

Abstract.

Rotary mechanical pulsation compensators require a torsionally compliant coupling attached to the pump rotor. To quantify their performance for different types of pumps, the pump outlet pressure magnitude minimum at the compensation frequency and the bandwidth of the compensation effect are considered. For these performance criteria, closed-form solutions are found with an undamped hydraulic oscillator or a simple capacitance at the pump outlet. Experiments are carried out with a compensator coupling and an internal gear pump attached to different hydraulic systems. Measurement results are compared with frequency domain response from appropriate theoretical models. Compensator performance is derived from experiments to validate closed-form solutions. Using these, pressure magnitude minimum and compensator bandwidth are predicted for an axial piston pump.

Keywords. Piston pump, gear pump, pressure pulsation, compensator coupling, pressure magnitude minimum, bandwidth.

1. INTRODUCTION

A novel pulsation compensation principle for hydraulic pumps and motors was introduced in [1]. This principle uses the mass moment of inertia of the machine rotor and requires a torsionally compliant coupling in the drivetrain. Assuming a suitable stiffness of such a coupling, numerical studies were provided in [2]. The design of a compensator coupling was described in [3], where the novel assembly was classified as rotary mechanical pulsation compensator. Measurements with a radial piston pump were presented in [4]. Although the desired effect could be demonstrated, better performance was expected for other types of pumps. In [2-4], theoretical predictions on compensator performance were made by plotting frequency response functions of the coupled hydraulic-mechanical system for particular sets of parameters.

In this paper, performance criteria for rotary mechanical pulsation compensators shall be specified. They address narrow-band pulsation compensation for constant speed applications and broadband pulsation reduction for relevant speed ranges. With respect to the attached hydraulic system, resonant and non-resonant conditions are distinguished. The coupled hydraulic-mechanical assembly is modelled by an analogue hydraulic system, which is transformed into a dual mechanical system [5] to apply the existing theory of mechanical vibration absorbers [6]. Closed-form solutions are derived for the relationships between system parameters and performance criteria. These solutions are verified by measurements on an internal gear pump attached to different hydraulic systems, which are compared to a coupled hydraulic-mechanical model in the frequency domain. Besides flow rate excitation as in previous models, torque excitation from geometric pulsation is also included. Finally, closed-form solutions are applied to predict compensator performance for an axial piston pump.

2. PERFORMANCE MEASURES

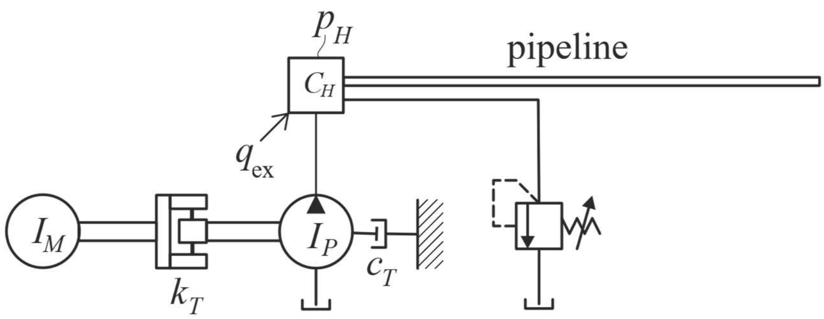

Figure 2.1. Schematic of setup with radial piston pump and pipeline

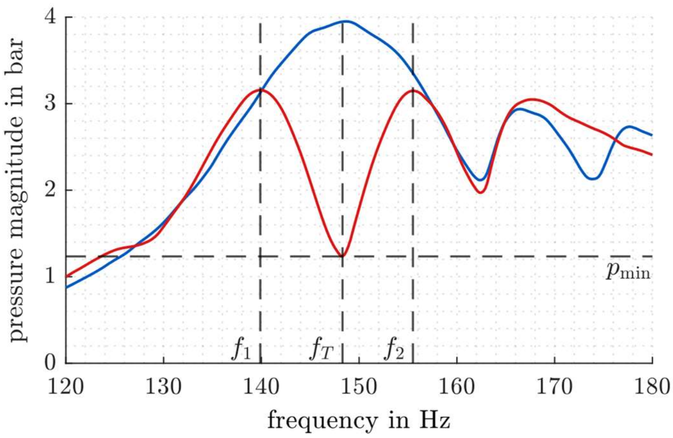

Figure 2.2. Pressure pulsations of radial piston pump. Blue: without compensator, red: with compensator

In [4], an assembly according to Figure 2.1 was used for first measurements on a rotary mechanical pulsation compensator. A compensator coupling with torsional stiffness k_T was arranged between the driving motor and a radial piston pump with mass moments of inertia I_M and I_P, respectively. The inevitable torsional damping on the pump rotor was denoted by c_T. Pump pulsations were considered as an external flow rate excitation q_{ex} into the hydraulic capacitance C_H at the pump outlet, which was connected to a pressure relief valve. A closed pipeline was attached at the pump outlet to obtain a hydraulic resonator. The pressure relief valve was known to be heavily damped with cut-off frequency far below the first pipeline resonance. In an alternative configuration, the compensator coupling was replaced by a comparatively stiff connection between the driving motor and the pump. The magnitudes of measured pressures p_H are shown in Figure 2.2. With compensator coupling, a minimum p_{min} occurred at the compensation frequency f_T between the side resonance frequencies f_1 and f_2.

Pulsation compensators can be used in different application cases. For constant speed applications, narrow-band compensation may be sufficient unless overshooting side resonances are passed during run-up or run-down. A range of pump speeds requires an appropriate bandwidth of the compensation effect. The pressure magnitude minimum p_{min} at the pump outlet constitutes an obvious performance criterion in all application cases. A second criterion is given by the compensator bandwidth $b = (f_2 - f_1)/f_T$, which roughly describes the pulsation reduction range. With respect to both criteria, compensator performance is rather limited for the radial piston pump. Therefore, pressure magnitude minimum and compensator bandwidth shall be analyzed for other types of pumps.

3. System Transformation

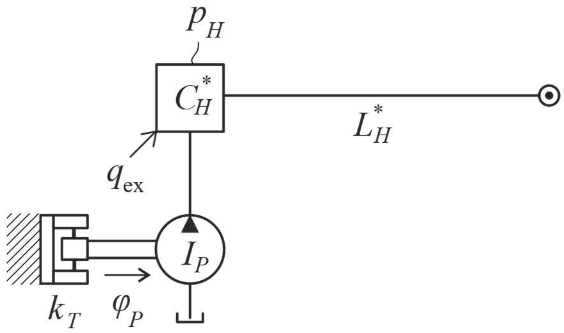

Figure 3.1. Coupled hydraulic-mechanical assembly with hydraulic oscillator

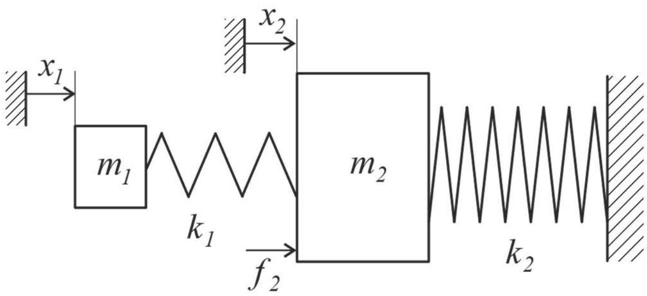

Figure 3.2. Dual mechanical system with fixed boundary

A simplified hydraulic-mechanical setup according to Figure 3.1 can be transformed into a mechanical system as follows. With the displacement V_P of the pump, the transmission ratio between the angle φ_P of the pump shaft and the displaced volume at the pump outlet is $2\pi/V_P$. In an analogue hydraulic system, the compliance of the compensator coupling becomes a hydraulic capacitance

$$C_T = \left(\frac{V_P}{2\pi}\right)^2 \frac{1}{k_T}, \tag{3.1}$$

and the pump inertia turns into a hydraulic inductance

$$L_T = \left(\frac{2\pi}{V_P}\right)^2 I_P. \tag{3.2}$$

Hydraulic capacitance C_H^* and hydraulic inductance L_H^* represent an undamped hydraulic oscillator at the pump outlet. The inductance L_H^* is connected to a constant pressure boundary. Considering the pressures

$$p_T = -\frac{2\pi}{V_P} k_T \varphi_P \tag{3.3}$$

and p_H as state variables, this hydraulic system corresponds to the dual mechanical system in Figure 3.2 with

$$m_1 = C_T \tag{3.4}$$

$$k_1 = \frac{1}{L_T} \tag{3.5}$$

$$m_2 = C_H^* \tag{3.6}$$

$$k_2 = \frac{1}{L_H^*} \tag{3.7}$$

and a fixed end boundary condition [5]. The state variables of the dual mechanical system are the velocities $\dot{x}_1 = p_T$ and $\dot{x}_2 = p_H$. It can be seen that the classical mechanical vibration absorber setting corresponds to a rotary mechanical pulsation compensator with resonant conditions of the attached hydraulic system.

Non-resonant conditions are obtained for a simple hydraulic capacitance at the pump outlet as shown in Figure 3.3. This setting corresponds to the dual mechanical system in Figure 3.4. With C_H instead of C_H^* Equations (3.1) to (3.6) still apply, free boundaries result, and state variables are defined as above.

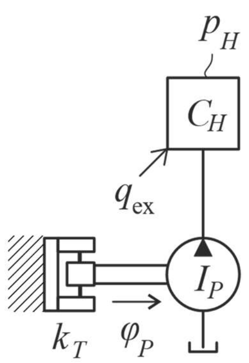

Figure 3.3. Coupled hydraulic-mechanical assembly with hydraulic capacitance

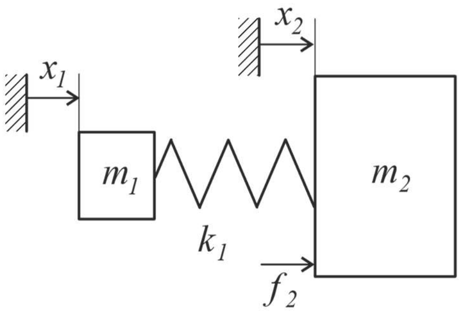

Figure 3.4. Dual mechanical system with free boundaries

4. CLOSED-FORM SOLUTIONS

For mechanical vibration absorbers, bandwidth considerations are available in [6]. Referring to Figure 3.2,

$$\frac{k_1}{m_1} = \frac{k_2}{m_2} \tag{4.1}$$

is assumed, which becomes

$$\frac{k_T}{I_P} = \frac{1}{C_H^* L_H^*} \tag{4.2}$$

with Equations (3.1 – 3.2) and (3.4 – 3.7). The bandwidth b of the absorber is obtained from the difference of the side resonance frequencies divided by the compensation frequency

$$f_T = \frac{1}{2\pi}\sqrt{\frac{k_1}{m_1}}. \tag{4.3}$$

An eigenvalue analysis of the system in Figure 3.2 yields the side resonance frequencies f_1 and f_2. With the mass ratio

$$\mu = \frac{m_1}{m_2}, \tag{4.4}$$

the bandwidth results as

$$b = \frac{f_2 - f_1}{f_T} = \sqrt{\frac{2+\mu+\sqrt{4\mu+\mu^2}}{2}} - \sqrt{\frac{2+\mu-\sqrt{4\mu+\mu^2}}{2}}. \tag{4.5}$$

For the hydraulic-mechanical assembly in Figure 3.1, Equations (3.1), (3.4), and (3.6) are used to calculate

$$\mu = \left(\frac{V_P}{2\pi}\right)^2 \frac{1}{k_T C_H^*}. \tag{4.6}$$

The compensator bandwidth b increases with μ, which means that the compensator coupling should be as compliant as possible.

For non-resonant conditions as in Figures 3.3 and 3.4, the lower side resonance does not exist. The compensator bandwidth can be calculated as

$$b_n = \frac{f_2\text{-}f_T}{f_T} = \sqrt{1+\mu}\text{-}1 \tag{4.7}$$

with μ according to Equations (4.4) or (4.6).

To determine the pump outlet pressure magnitude minimum p_{min} under resonant conditions as in Figure 3.1, torsional damping c_T on the pump rotor must be taken into account. According to the assumption (4.2), the attached hydraulic system is capable of autonomous pulsations at the compensation frequency

$$f_T = \frac{1}{2\pi}\sqrt{\frac{k_T}{I_P}}. \tag{4.8}$$

The remaining torsional single-degree-of-freedom oscillator yields the relationship

$$(\text{-}\omega^2 I_P + i\omega c_T + k_T)\frac{2\pi}{V_P}Q_{ex}(i\omega) = \text{-}i\omega\frac{V_P}{2\pi}P_H(i\omega) \tag{4.9}$$

with the angular frequency ω and the Laplace Transforms Q_{ex} and P_H of q_{ex} and p_H, respectively. At $\omega = \omega_T = 2\pi f_T$, this becomes

$$P_H(i\omega_T) = \text{-}c_T\left(\frac{2\pi}{V_P}\right)^2 Q_{ex}(i\omega_T). \tag{4.10}$$

For the fundamental harmonic of the flow rate excitation,

$$Q_{ex}(i\omega_T) = \frac{V_{ex}}{2\pi}\cdot\frac{\omega_T}{z} \tag{4.11}$$

results with the displacement amplitude V_{ex} and the number z of pulsations per revolution of the pump shaft. As the pressure magnitude minimum will occur near $\omega = \omega_T$,

$$p_{min} \approx \frac{2\pi\omega_T c_T V_{ex}}{z V_P^2} \tag{4.12}$$

is obtained as an approximation.

Under non-resonant conditions, it is possible to calculate a pressure magnitude reduction compared to the pressure magnitude p_C resulting form the flow rate excitation q_{ex} into the closed hydraulic capacitance C_H. For the assembly in Figure 3.3, it can be shown that

$$\frac{p_{min}}{p_C} \approx \frac{1}{\sqrt{1+\frac{1}{\left(C_H\left(\frac{2\pi}{V_P}\right)^2\omega_T c_T\right)^2}}}. \tag{4.13}$$

Apparently, the torsional damping on the pump rotor should be as small as possible.

5. EXPERIMENTS WITH INTERNAL GEAR PUMP

The existing compensator coupling is combined with an internal gear pump and different hydraulic systems at the pump outlet. Figure 5.1 shows the experimental setup. The drivetrain consists of an electric motor, a torque measurement shaft, the compensator coupling, and the internal gear pump. The pipeline at the pump outlet can be closed at different lengths or disconnected completely. The mean pressure is adjusted by a pressure relief valve. The compensator coupling is realized by a spoke wheel according to Figure 5.2, which also shows one of the rotation angle sensors mounted on each side of the compensator coupling.

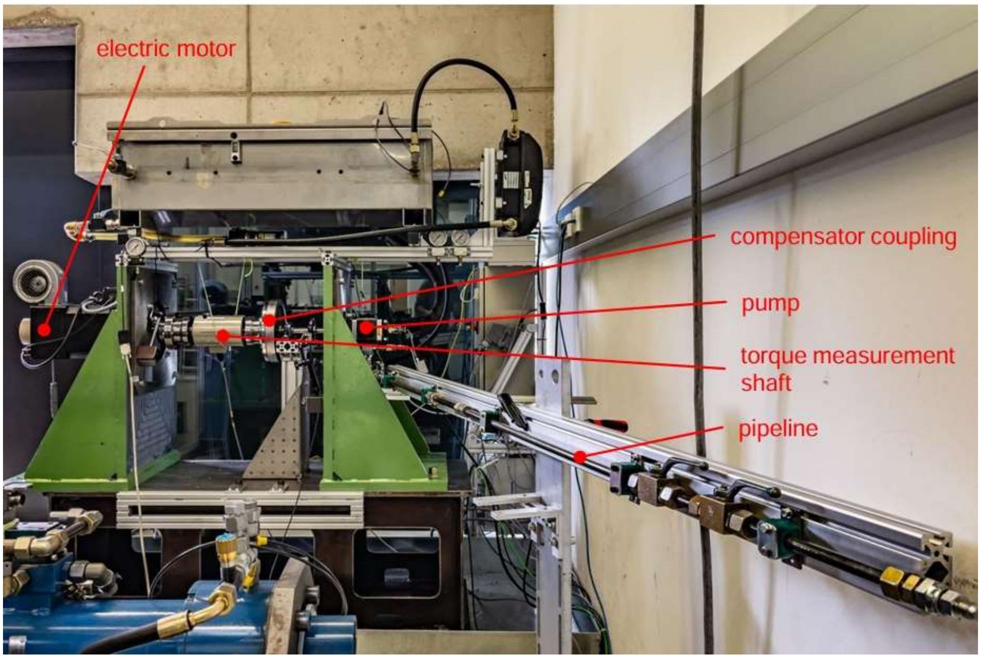

Figure 5.1. Experimental setup

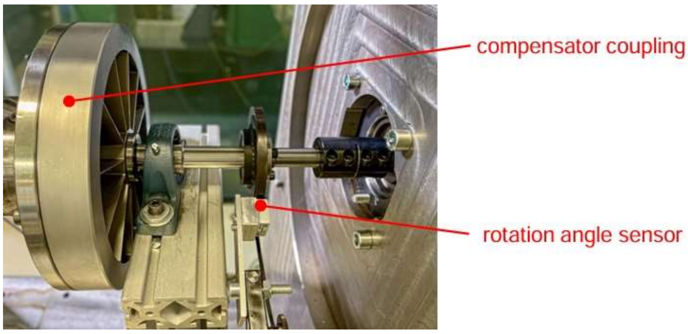

Figure 5.2. Detail with compensator coupling

The hydraulic systems at the pump outlet consist in pipelines of different lengths and the inevitable capacitance of the fittings between pump, pressure relief valve, pressure sensor, and pipeline attachment. If the pipeline is disconnected, this capacitance remains. The rotational speed of the driving motor is increased stepwise from 500 to 2000 rpm. Ten full rotations are performed after each step of 4 rpm. For each rotational speed, rectangular windows of measured signals are considered with a trigger on the pump shaft angle, and Fourier coefficients of the fundamental pulsation frequency are calculated. In this way, the phase with respect to flow rate excitation can also be obtained. All experiments are repeated without compensator coupling.

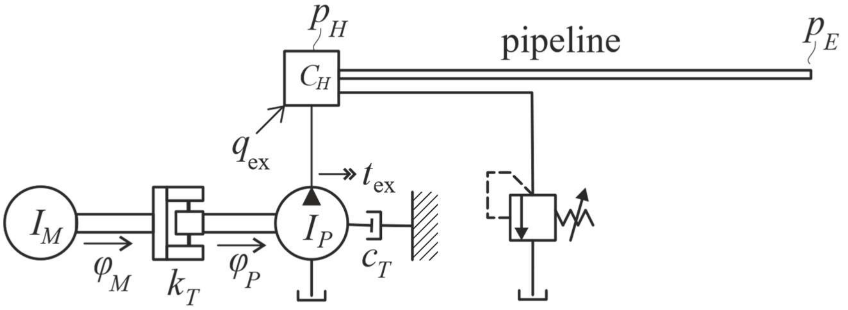

Figure 5.3. Schematic of setup with internal gear pump and pipeline

The coupled hydraulic-mechanical model in Figure 5.3 is implemented for comparison with measurements. In addition to previous models, an excitation torque t_{ex} is considered on the pump rotor. This excitation applies for geometric pulsations and originates from the fluctuating transmission ratio between the mean pressure and the torque on the pump rotor, which is determined by the respective displacement amplitude $V_{ex,g}$. In contrast, dynamic pulsations do not imply an excitation torque and only contribute a flow rate excitation.

Flow rate pulsations of external gear pumps have been studied extensively [7]. Comparable information on internal gear pumps can be found for a particular tooth profile [8]. It is concluded from literature that for both types of gear pumps, geometric and dynamic pulsations can be relevant. Therefore, q_{ex} and t_{ex} are considered as independent excitations.

The model further includes the dynamic behavior of the pipeline and the resistance R of the pressure relief valve. It is assumed that this resistance depends on the mean flow rate, which is proportional to the fundamental pulsation frequency. The state variables of the model are the rotation angles φ_M and φ_P on motor and pump side of the compensator coupling, the pressure p_H at the pump outlet, and the pressure p_E at the closed end of the pipeline. The respective Laplace transforms are denoted by Φ_M, Φ_P, P_H, and P_E, while Q_{ex} and T_{ex} denote the Laplace transforms of flow rate excitation and excitation torque, respectively.

In the frequency domain, the model can be formulated as

$$\left(-\omega^2\begin{bmatrix} I_M & 0 & 0 & 0 \\ 0 & I_P & 0 & 0 \\ 0 & -\frac{V_P}{2\pi} & C_H & 0 \\ 0 & 0 & 0 & 0 \end{bmatrix} + i\omega\begin{bmatrix} 0 & 0 & 0 & 0 \\ 0 & c_T & 0 & 0 \\ 0 & 0 & \frac{1}{R(i\omega)} + S(i\omega) & T(i\omega) \\ 0 & 0 & T(i\omega) & S(i\omega) \end{bmatrix} + \begin{bmatrix} k_T & -k_T & 0 & 0 \\ -k_T & k_T & \frac{V_P}{2\pi} & 0 \\ 0 & 0 & 0 & 0 \\ 0 & 0 & 0 & 0 \end{bmatrix}\right)\begin{bmatrix} \Phi_M(i\omega) \\ \Phi_P(i\omega) \\ P_H(i\omega) \\ P_E(i\omega) \end{bmatrix} = \begin{bmatrix} 0 \\ T_{ex}(i\omega) \\ i\omega Q_{ex}(i\omega) \\ 0 \end{bmatrix} \tag{5.1}$$

with the functions

$$S(i\omega) = -\frac{iA}{\sqrt{E\rho}\,f(i\omega)} \cdot \cot\left(\frac{f(i\omega)\omega l}{\sqrt{E/\rho}}\right) \tag{5.2}$$

and

$$T(i\omega) = \frac{iA}{\sqrt{E\rho}\,f(i\omega)} \cdot 1/\sin\left(\frac{f(i\omega)\omega l}{\sqrt{E/\rho}}\right) \tag{5.3}$$

describing the dynamic behaviour of the pipeline with

$$f(i\omega) = \sqrt{-\frac{J_0(ir\sqrt{i\omega/\nu})}{J_2(ir\sqrt{i\omega/\nu})}}, \tag{5.4}$$

where J_0 and J_2 are Bessel functions of first kind [9]. For an internal gear pump, the fundamental frequencies of geometric and dynamic pulsations coincide and the corresponding angular frequency is denoted by ω. The resistance model is formulated as

$$R(i\omega) = p_{ref}/\left(\frac{V_P}{2\pi} \cdot \frac{\omega}{z}\right), \tag{5.5}$$

where pump leakage is considered by choosing the reference pressure p_{ref} higher than the pump outlet pressure. In the frequency domain, the flow rate excitation from geometric pulsations reads

$$Q_{ex,g}(i\omega) = \frac{V_{ex,g}}{2\pi} \cdot \frac{\omega}{z}, \tag{5.6}$$

in which z is the number of teeth of the gear on the pump shaft. The corresponding excitation torque becomes

$$T_{ex}(i\omega) = -\frac{V_{ex,g}}{2\pi} \cdot p_m, \tag{5.7}$$

where p_m denotes the mean pressure at the pump outlet. In an operating point, the flow rate excitation from dynamic pulsations can be written as

$$Q_{ex,d}(i\omega) = \frac{V_{ex,d}}{2\pi} \cdot \frac{\omega}{z} \cdot e^{i\alpha} \tag{5.8}$$

in analogy to Equation (5.6) with a phase shift α which is assumed to be frequency independent for simplicity. Then, the total flow rate excitation becomes

$$Q_{ex}(i\omega) = Q_{ex,g}(i\omega) + Q_{ex,d}(i\omega) = \frac{V_{ex}}{2\pi} \cdot \frac{\omega}{z} \cdot e^{i\beta} \tag{5.9}$$

with a resulting phase shift β.

Model parameters are summarized in Table 1. For the reference case without compensator coupling, a rigid connection of electric motor and pump is assumed so that the angles φ_M and φ_P coincide. In this case, the excitation torque t_{ex} acts directly on a high mass moment of inertia with negligible effect on the resulting motion. Therefore, the parameter V_{ex} could be identified by comparing measured and calculated pressure magnitude maxima under resonant conditions of the hydraulic system. With compensator coupling, the parameters I_P, c_T, $V_{ex,g}$, and β have been adjusted by respective comparisons of compensation frequencies, pump outlet pressure magnitudes at compensation and side resonance frequencies, and phase curves of the pump outlet pressure.

Table 5.1. Model parameters

motor sided mass moment of inertia	I_M	0.16 kg m^2
compensator coupling stiffness	k_T	2350 Nm/rad
pump sided mass moment of inertia	I_P	0.0008 kg m^2
pump displacement	V_P	25 cm^3
number of teeth	z	13
total displacement amplitude	V_{ex}	0.025 V_P
geometric pulsation displacement amplitude	$V_{ex,g}$	0.0125 V_P
phase shift	β	80°
torsional damping constant	c_T	0.01 Nms/rad
dead volume at pump outlet	V_d	1.8 V_P
bulk modulus	E	16000 bar
hydraulic capacitance at pump outlet	C_H	V_d/E
reference pressure	p_{ref}	150 bar
mean pressure	p_m	100 bar
pipeline length	l	221 / 189 cm
pipeline radius	r	6 mm
fluid density	ρ	870 kg/m^3
kinematic viscosity	υ	50 mm^2/s

In addition to the pressure p_H at the pump outlet, a torque equivalent pressure

$$p_T = \frac{2\pi}{V_P} k_T(\varphi_M - \varphi_P) \tag{5.10}$$

in the compensator coupling is considered in both measurements and calculations. Frequency domain measurements for 221 cm pipeline length are shown in Figure 5.4. Figure 5.5 shows the respective calculations. The blue curves apply for the case without compensator coupling, where the torque equivalent pressure cannot be calculated. With compensator coupling, the torque equivalent pressure p_T reaches much higher values than the pressure p_H at the pump outlet and is therefore downscaled by a factor of 5. Measured and calculated pressures match fairly well, which is also the case for 189 cm pipeline length (see Figures 5.6 and 5.7).

For 221 cm pipeline length, the compensation frequency and the resonance frequency of the hydraulic system coincide at 258 Hz, which corresponds to a pump speed of 1191 rpm. With compensator coupling, both measurement and model result in a pump outlet pressure magnitude minimum of 0.15 bar, which corresponds to a reduction to 5 % of the magnitude without compensator coupling. The closed-form solution (4.12) yields a value of 0.083 bar. This solution does not account for the excitation torque, which explains the deviation from the measured value. It should be noted that the closed-form solution relies on the identified displacement amplitude V_{ex} and the adjusted torsional damping constant c_T.

According to measurements, the compensator bandwidth amounts to 24 %, while 27 % are obtained from the model. Increasing the dead volume V_d by a third of the pipeline volume to estimate the hydraulic capacitance C_H^* in Equation (4.6), the closed-form solution (4.5) for the bandwidth becomes 29 %, which is in fair agreement with measurements.

The compensator exhibits excellent performance at the compensation frequency and is robust with respect to small variations in pump speed. However, an overshooting upper side resonance occurs, and the respective pulsation frequencies should be avoided.

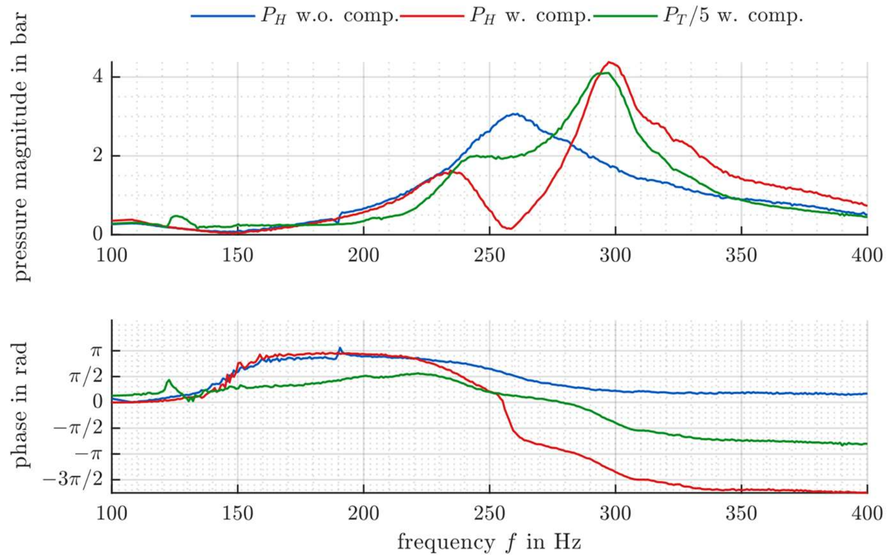

Figure 5.4. Measured pressures for 221 cm pipeline length

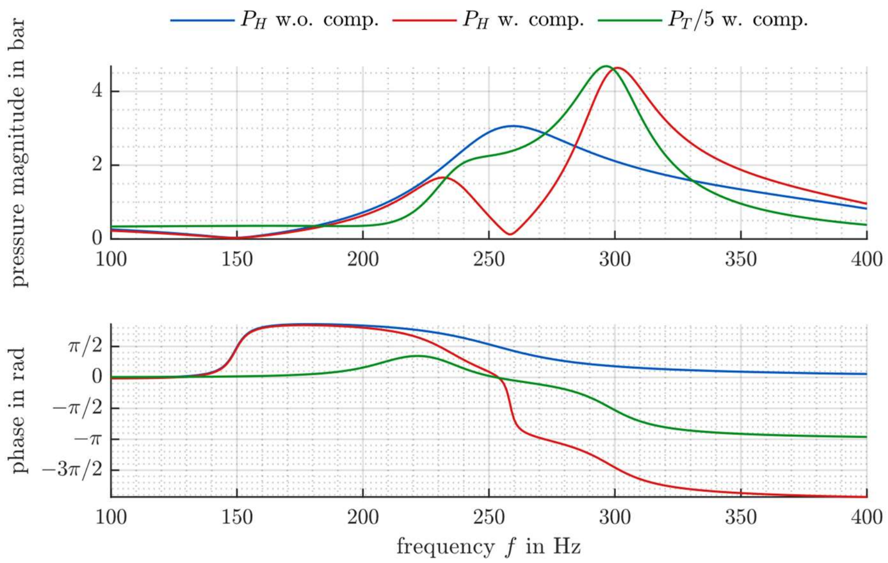

Figure 5.5. Calculated pressures for 221 cm pipeline length

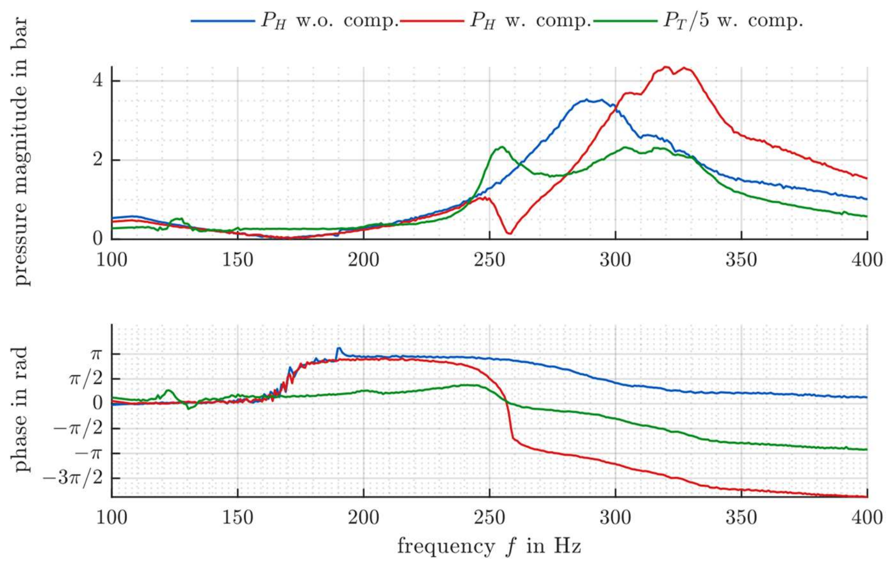

Figure 5.6. Measured pressures for 189 cm pipeline length

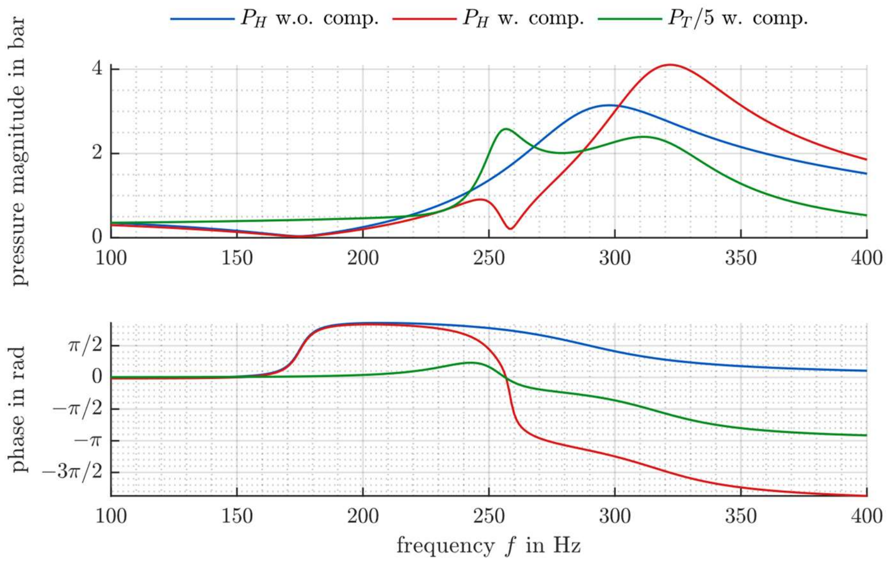

Figure 5.7. Calculated pressures for 189 cm pipeline length

By reducing the pipeline length to 189 cm, the resonance frequency of the hydraulic system is increased and no longer coincides with the compensation frequency. Around the compensation frequency, the compensator still reduces the pump outlet pressure magnitude.

Condition (4.2) is no longer fulfilled so that the closed-form solutions are not applicable in this case.

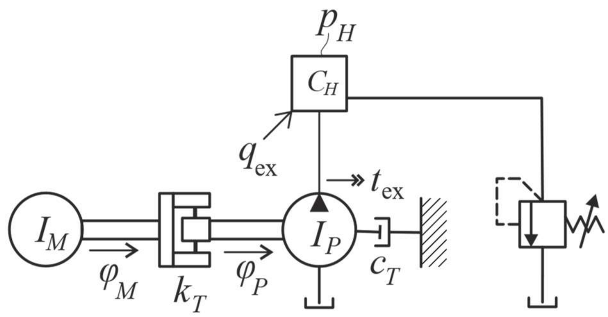

Figure 5.8. Schematic of setup with internal gear pump and outlet capacitance

If the pipeline is disconnected from the pump outlet, the model in Figure 5.8 applies. The respective frequency domain formulation reads

$$\left(-\omega^2 \begin{bmatrix} I_M & 0 & 0 \\ 0 & I_P & 0 \\ 0 & -\frac{V_P}{2\pi} & C_H \end{bmatrix} + i\omega \begin{bmatrix} 0 & 0 & 0 \\ 0 & c_T & 0 \\ 0 & 0 & \frac{1}{R(i\omega)} \end{bmatrix} + \right.$$

$$\left. + \begin{bmatrix} k_T & -k_T & 0 \\ -k_T & k_T & \frac{V_P}{2\pi} \\ 0 & 0 & 0 \end{bmatrix} \right) \begin{bmatrix} \Phi_M(i\omega) \\ \Phi_P(i\omega) \\ P_H(i\omega) \end{bmatrix} = \begin{bmatrix} 0 \\ T_{ex}(i\omega) \\ i\omega Q_{ex}(i\omega) \end{bmatrix}. \quad (5.11)$$

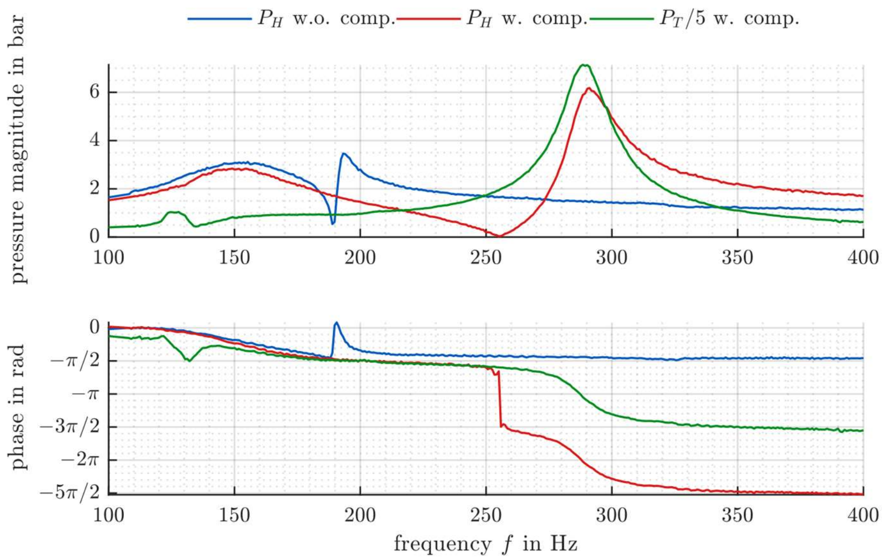

Figure 5.9. Measured pressures with outlet capacitance

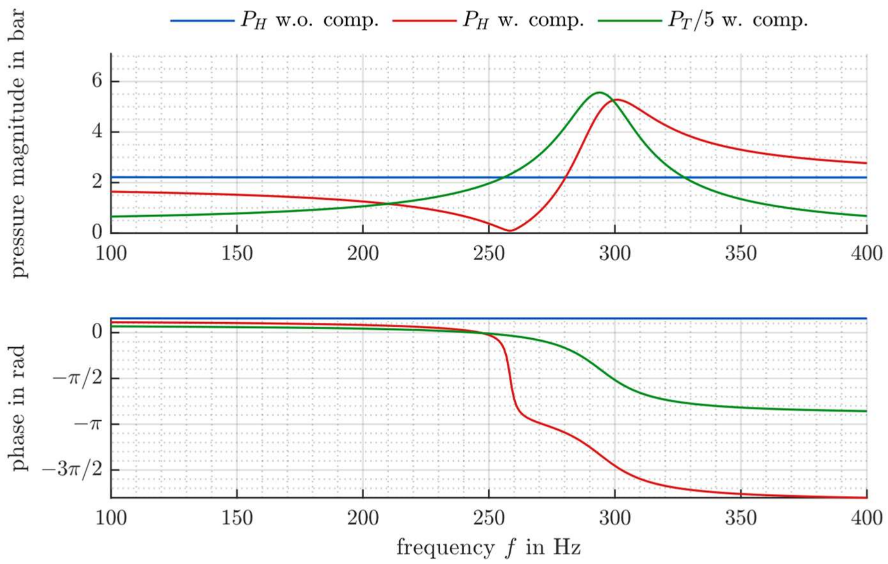

Figure 5.10. Calculated pressures with outlet capacitance

Figure 5.9 shows the corresponding measurements. Around 190 Hz, they contain an additional effect from the torque measurement shaft, which is not included in the model. Calculated results are shown in Figure 5.10. At the compensation frequency, the pump outlet pressure magnitude is almost cancelled. The closed-form solution (4.13) results in a pressure magnitude reduction to 3 %. There is no lower side resonance, and broadband pulsation reduction is achieved below the compensation frequency. Above this frequency, a heavily overshooting side resonance is observed. The measured bandwidth amounts to 13.7 %, and the frequency domain model yields a bandwidth of 16.7 %. For comparison, the closed-form solution (4.7) results in a bandwidth of 11.3 %.

6. PREDICTIONS FOR AXIAL PISTON PUMP

Under non-resonant conditions, closed-form solutions for compensator performance shall be evaluated for an axial piston pump with seven pistons, 25 cm^3 displacement, and 0.0017 kg m^2 mass moment of inertia at a rotational speed of 1500 rpm. In a first approach, the hydraulic capacitance at the pump outlet and the torsional damping constant are taken from the internal gear pump with the same displacement. The compensator is tuned to the fundamental frequency of dynamic pulsations, which occurs at 175 Hz. Equation (4.8) can be used to calculate the required torsional stiffness of the compensator coupling. With Equation (4.6), Equation (4.7) yields a bandwidth of 12.9 %. Equation (4.13) results in a pressure magnitude reduction to 2.0 %. At 3000 rpm, a bandwidth of 3.4 % and a pressure magnitude reduction to 3.9 % are obtained. Smaller bandwidth is due to higher stiffness of the compensator coupling required for 350 Hz compensation frequency. If damping is increased by a factor of five, pressure magnitude reductions to 9.7 % and 19.2 % result for 1500 rpm and 3000 rpm, respectively.

7. Conclusions

For the investigated internal gear pump, the rotary mechanical pulsation compensator shows excellent performance at a mean outlet pressure of 100 bar and a constant rotational speed near 1200 rpm. Due to sufficient bandwidth, it is robust with respect to small speed variations. Similar performance is expected from an equally sized axial piston pump at a rotational speed of 1500 rpm. At higher pump speeds, the remaining pulsation will be higher and the bandwidth will decrease.

For external gear pumps, geometric pulsations may dominate and cause a significant excitation torque. In this case, the closed-form solutions for compensator performance are no longer applicable. Appropriate investigations of external gear pumps will be presented in the future.

8. References

[1] G. Mikota, 'Vorrichtung zur Reduktion von Druckpulsationen in einem Hydraulik-system', Austrian Patent AT 526449 B1 2024-05-15.

[2] G. Mikota, B. Manhartsgruber, 'A novel pulsation compensator for displacement machines', Proc. 14th International Fluid Power Conference (14th IFK), pp. 395-406, Dresden, 19th – 21th March, 2024.

[3] G. Mikota, 'Design and simulation of a drivetrain integrated pulsation compensator for pumps', Proc. BATH/ASME 2024 Symposium on Fluid Power and Motion Control (FPMC 2024), FPMC2024-140002, Bath, 11th – 13th Sept., 2024.

[4] D. Holzer, G. Mikota, 'Measurement of a rotary mechanical pulsation compensator under hydraulic resonance', Proc. 19th Scandinavian International Conference on Fluid Power (SICFP'25), Paper No. 43, Linköping, 2nd – 4th June, 2025.

[5] G. Hametner, R. Scheidl, 'Duality and its application for the dynamic analysis of hydraulic drive systems', Proc. Bath Workshop on Power Transmission and Motion Control (PTMC 2003), pp. 65-76, Bath, 10th – 12th Sept., 2003.

[6] H. Dresig, F. Holzweißig, 'Dynamics of Machinery', Springer, 2010.

[7] X. Zhao, A. Vacca, 'Theoretical investigation into the ripple source of external gear pumps', Energies 12 (2019) 535.

[8] H. Chai, G. Yang, G. Wu, G. Bai, W. Li., 'Research on flow characteristics of straight line conjugate internal meshing gear pump', Processes 8 (2020) 269.

[9] H. Theißen, 'Die Berücksichtigung instationärer Rohrströmung bei der Simulation hydraulischer Anlagen', Dissertation, RWTH Aachen, 1984.

Biographies

Gudrun Mikota received the diploma in mechanical engineering from Vienna University of Technology in 1994, the doctorate in mechanical engineering from Vienna University of Technology in 2001, and the habilitation in dynamics of machines from Johannes Kepler University Linz in 2021. She has worked with companies Jenbacher, LCM, and Eisenbeiss. In 2023, she was appointed Professor of Fluid Power at Johannes Kepler University Linz. Her research areas include fluid power dynamics, modal analysis of hydraulic and rotating systems, energy efficient hydraulic drives, and the dynamic behaviour of the human arterial system.

David Holzer received the bachelor's degree in mechatronics from Johannes Kepler University Linz in 2021 and the master's degree in mechatronics from Johannes Kepler University Linz in 2023. He is currently working as a Scientific Assistant at the Institute of Machine Design and Fluid Power, Johannes Kepler University Linz. His research area is the dynamic behaviour of efficient hydraulic machinery.